



The thermophysical properties of a promising composite adsorbent based on multi-wall carbon nanotubes for heat storage

Alexandra Grekova¹ · Svetlana Strelova¹ · Marina Solovyeva¹ · Mikhail Tokarev¹

Received: 14 August 2023 / Accepted: 3 November 2023 / Published online: 24 January 2024
© The Author(s) 2024

Abstract

The use of energy from alternative energy sources as well as the use of waste heat are key elements of an efficient energetics. Adsorption heat storage is a technology that allows solving such problems. For the successful operation of an adsorption heat accumulator, it is necessary to analyze the thermophysical characteristics of the system under the conditions of the operating cycle: heat transfer coefficient adsorbent-metal (α_2), overall (U) and global (UA) heat transfer coefficients of heat exchanger. Multi-walled carbon nanotube (MWCNT) composites are very promising for adsorption-based renewable energy storage and conversion technologies. In this work at the stage of heat release, α_2 was measured by the large pressure jump (LPJ) method, at the stage of heat storage by large temperature jump method (LTJ), which made it possible to obtain thermophysical characteristics that corresponded to the implementation of the real working cycle as much as possible. The heat transfer coefficients for a pair of adsorbent LiCl/MWCNT—methanol are measured for the first time under the conditions of a daily heat storage cycle both at the sorption stage ($\alpha_2 = 190 \text{ W/m}^2\text{K}$) and at the desorption stage ($\alpha_2 = 170 \text{ W/m}^2\text{K}$).

Keywords Energy saving · Multi-wall carbon nanotubes · Adsorption heat storage · Heat transfer coefficient · Pressure jump · Methanol sorption

Abbreviations

AHS	Adsorption heat storage
FFT	Finned flat tube
LPJ	Large pressure jump
LTJ	Large temperature jump
MWCNT	Multi-wall carbon nano tubes
HTF	Heat transfer fluid
AdHex	Adsorber heat exchanger

List of Symbols

A	Area, m^2
D	Coefficient
Q	Coefficient
E	Efficiency of the fin
F	Adsorption potential, $\text{J}/(\text{molK})$
h	Height, m
H	Enthalpy, J/g
ΔH	Isosteric heat, J/mol
H^0	Enthalpy of evaporation, J/mol
K	Finning coefficient

m	Mass, g
Nu	Nusselt number
P	Pressure, bar
q	Conversion
R	Universal gas constant, $8.31 \text{ J}/(\text{molK})$
S	Surface area, m^2
T	Temperature, K , $^\circ\text{C}$
t	Time, s
U	Overall heat transfer coefficient, $\text{W}/(\text{m}^2\text{K})$
UA	Global heat transfer coefficient, W/K
V	Volume, dm^3
W	Specific power, W/g
w	Uptake, g/g

Superscripts

ad	Adsorption
con	Condenser, condensation
ch	Channel
d	Desorption
ev	Evaporator, evaporation
f	Fin
fin	Final
HEX	Heat exchanger
init	Initial
max	Maximum

✉ Alexandra Grekova
grekova@catalysis.ru

¹ Boreskov Institute of Catalysis, Lavrentiev Ave. 5,
Novosibirsk 630090, Russia

min	Minimum
reg	Regeneration
w	Wall
0	Saturation
*	Equilibrium
1	Media 1
2	Media 2

Greek symbols

α	Heat transfer coefficient, $W/(m^2K)$
δ	Thickness
Δ	Difference, distance
λ	Thermal conductivity, $W/(mK)$
τ	Characteristic time, s

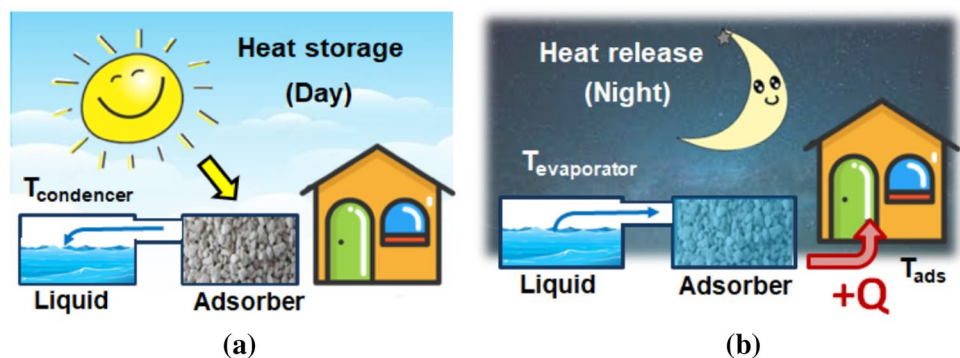
Introduction

The environmental situation on the planet is becoming a growing concern for the global community with each passing year [1]. A significant part of environmental problems is related to the use of non-renewable energy sources and atmospheric pollution by the products of their combustion [2]. Due to population growth, as well as global urbanization and the expansion of factories and cities, the problems mentioned are becoming more and more acute every year [3]. To solve them, it is important to overcome challenges in several directions: (1) the use of alternative energy sources [4]; (2) the reuse of waste heat in industry, transport and housing sector [5, 6]. The main difficulty in using such energy sources is the inconsistency in time between the processes of heat generation and consumption [7]. However, developments in both the first and second directions can be implemented using the technology of adsorption heat storage (AHS) [8, 9]. In comparison with sensible [10, 11], and latent heat storage [12, 13] the AHS can be characterized by higher heat storage capacity and negligible losses during the heat storage stage [14]. This energy-saving technology solves the problem of harmonization between the stages of generation and consumption of waste heat. The

main elements of an adsorption heat accumulator are a vessel with a working liquid and an adsorber-heat exchanger (AdHex) filled with an adsorbent (Fig. 1). Due to their porous structure and chemical nature, adsorbents are able to reversibly bind vapors of the working fluid. The sorption/desorption processes are accompanied by exothermic/endo-thermic thermal effects, which can be used by the consumer. Another advantage of the adsorption heat storage technology is the possibility to use low-grade heat (for example, solar and geothermal energy, waste heat from engines of various mechanisms, etc.) with a temperature potential of less than $100\text{ }^\circ\text{C}$ for adsorbent regeneration [15]. Let us consider the working principle of an adsorption heat accumulator for the process of daily heat storage [16]. The adsorbent is dried due to the Sun energy harvested by a solar collector of the simplest design which can provide regeneration temperature (T_{reg}) about $80\text{ }^\circ\text{C}$. At the same time, the desorbed vapors of the working fluid are collected in the condenser, which is at ambient temperature during the day (T_{con}) (Fig. 1). After drying, the adsorbent must be isolated from the reservoir with the working liquid using a system of taps—the accumulated heat can be stored indefinitely. If there is a need to release and use the stored heat, it is necessary to bring the dry adsorbent into contact with the vapors of the working fluid maintained at the evaporation temperature T_{ev} —heat will be released due to the implementation of the exothermic sorption process at the desired temperature T_{ad} .

The thermodynamic cycle of daily adsorption heat accumulation is determined by four stages presented in Clausius–Clapeyron coordinates (Fig. 2). The stage of adsorbent regeneration 1–2 is realized at constant pressure in the condenser P_{con} . During this stage a certain amount of working liquid Δw is desorbed from adsorbent and collected in the condenser. This process requires the supply of a certain amount of heat sufficient to desorb the vapors and heat up the adsorbent. Isosteric cooling of the adsorbent 2–3 proceeds when the adsorbent is disconnected from the reservoir with the working fluid and amount w_{min} of working liquid associated with the adsorbent is unchanged.

Fig. 1 Principle of **a** adsorption stage; **b** desorption stage



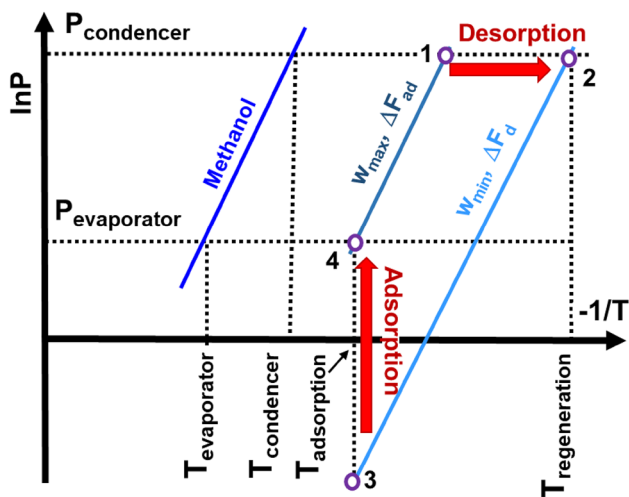


Fig. 2 Working cycle of adsorption heat storage process

The stage of heat release 3–4 is initiated by a sharp change in pressure over the adsorbent up to P_{ev} . During this stage the vapors of the working liquid that was desorbed at (1–2) come from the reservoir back to the adsorber where useful heat is released due to adsorption. The final stage of the considered cycle is isosteric heating (at constant uptake w_{max}) of the adsorbent prior to regeneration 4–1. At this stage some heat is required to heat up the adsorbent.

The perfection of such kind of adsorption heat accumulator can be determined by a set of different criteria, among which one can mention the following: (1) the amount of stored heat per unit mass or volume; (2) balance between the useful heat obtained at the adsorption stage and heat consumed for regeneration; (3) the intensity of heat release and heat consumption at these two stages. The first two criteria are determined mainly by thermodynamic properties of the adsorbent whereas the intensity of heat transfer depends on conductance of AdHex unit. That is why, knowledge of these properties is of a great importance for improvement of the AdHex, that is one of the most important opportunities for increasing the efficiency of the adsorption heat machine [17, 18]. Currently, finned flat tube (FFT) heat exchangers are used to design real prototypes and laboratory test rigs [19]. A number of works have shown that FFT geometry is the most promising for the applications under consideration [20]. The intensity of heat transfer in the adsorbent–heat exchanger system is characterized by global heat transfer coefficient (UA) of the heat exchanger. The UA coefficient is a function of heat transfer coefficient α_2 between the metal and the adsorbent and geometric parameters of AdHex [21]. The change in α_2 coefficient can dramatically affect the UA value of the system. The method of large temperature jump (LTJ) [22] is a powerful technique for measuring the α_2 coefficient. However, this method is widely used for adsorption

cycles, where both the regeneration (desorption) and cold production (adsorption) stages are isobaric [23]. Previously, it was shown that when using α_2 obtained by the LTJ method as parameter for calculating UA, the result of the calculation and the results of direct measurement of UA for the FFT heat exchanger are very close [24].

In the cycle under consideration, the heat storage stage (1–2 Fig. 2) is initiated by sharp temperature jump whereas heat release stage is initiated by sharp pressure jump (3–4 Fig. 2). Thus, the target adsorption stage is not isobaric, but, initiated by change in pressure over the adsorbent. Considering, in general, the state of the art in the field of adsorption systems of heat conversion and storage, [25, 26] one can say that the luggage of knowledge about the properties of adsorbents is richer in knowledge about their thermodynamic properties than about their dynamic data. That is why in this work, the measurements of the metal–adsorbent heat transfer coefficients are carried out not only by the standard LTJ technique applicable to the regeneration stage, but also by a new technique specialized for heat release stage under pressure jump conditions. This is of fundamental importance, since such technique simulates how the stage of heat release occurs under the conditions of the cycle. The paper will consider the cycle of daily heat storage during the off-season ($T_{con} = 15^\circ\text{C}$, $T_{ev} = 5^\circ\text{C}$, $T_{reg} = 80^\circ\text{C}$, $T_{ad} = 30^\circ\text{C}$). The composites “Salt inside porous matrix” are very promising for adsorption heat transformation [27]. Modification of porous matrix by active salt increases sorption capacity of the material [23]. For example, lithium chloride is very popular for synthesis of composite sorbents for adsorption heat transformers [28, 29]. In this work a promising system of composite adsorbent based on multi-wall carbon nanotubes—methanol was chosen as a working pair. Nanotubes are widely used to create various composite materials [30, 31], including composite adsorbents for adsorption applications [32–34]. It has been shown that using of such materials with stepped adsorption isotherm is very profitable for adsorption heat storage, both from the thermodynamic (high sorption capacity under the conditions of adsorption heat storage cycles [33, 35]) and from the dynamic point of view [36] (high power values both at the sorption stage and at the regeneration stage [37]). It was shown that the composite demonstrates heat storage capacity up to 0.92 kJ/g even at very low regeneration temperature 70–80 °C [33] which can be supported by simplest solar collector.

For many composite materials, the literature presents data on sorption equilibrium and energy storage capacity under the conditions of adsorption heat transformation cycles [16]. However, for the implementation of adsorption heat transformers into real life, it is necessary to study not only the thermodynamic but also the thermophysical characteristics of sorbents. In this work, for the first time, heat transfer coefficients sorbent–metal will be measured for the “LiCl/

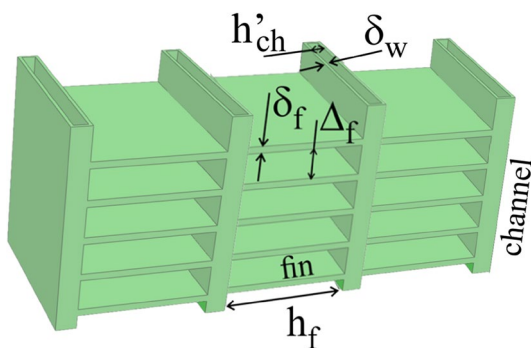


Fig. 3 Scheme of fins and channels of FFT heat exchanger

MWCNT—methanol” system based on multi-wall carbon nanotubes (MWCNT) both for the sorption and for the desorption stages of the adsorption heat storage cycle. Using measured α_2 global heat transfer coefficients for FFT heat exchanger will be calculated. These data are important both from practical and fundamental points of view.

Theoretical considerations

In FFT heat exchanger, the granules of adsorbent are placed between the fins and the channels through which the heat transfer fluid (HTF) circulates (Fig. 3).

The global heat transfer coefficient UA for FFT heat exchangers can be calculated as a product of the overall heat transfer coefficient U (W/m^2K) by the channels area A . The overall heat transfer coefficient can be expressed according to the formula [38, 39]:

$$U = \left[\frac{1}{\alpha_1} + \frac{\delta_w}{\lambda_w} + \frac{1}{\alpha_2(1 + E(K - 1))} \right]^{-1} \tag{1}$$

where λ_w is the thermal conductivity of the channel’s wall ($\lambda_w = 200$ $W/(mK)$ for aluminum), δ_w is the thickness of the channel’s wall, α_1 is heat transfer coefficient between HTF and channel’s wall, α_2 heat transfer coefficient between granules of the adsorbent and metal of Hex, E fin efficiency coefficient, K finning coefficient [38].

Parameter E characterizes how heat removal from fin’s surface decreases due to the non-isothermal nature of the real thin fin compared to the ideal case, if the fin was completely isothermal [38]:

$$E = \frac{\tanh(0.5h_f \sqrt{2\alpha_2/\delta_f \lambda_w})}{0.5h_f \sqrt{2\alpha_2/\delta_f \lambda_w}} \tag{2}$$

where δ_f is the thickness of the fin, λ_w is the thermal conductivity of metal. The α_1 coefficient between the channel’s

wall and the HTF depends on the geometry of the channels and the physical properties of the fluid:

$$\alpha_1 = \frac{Nu \cdot \lambda_{HTF}}{h'_{ch}} \tag{3}$$

where, h'_{ch} is the internal channel’s height, λ_{HTF} is the thermal conductivity of HTF (for water $\lambda_{HTF} = 0.67$ W/mK at $80^\circ C$ and 0.618 W/mK at $30^\circ C$), Nu is the Nusselt number. In case of laminar flow the Nusselt number realized for discussed geometry equals about 8 [40]. To find the α_2 coefficients, measurements under the realistic conditions of the considered working cycle should be carried out (Fig. 4).

For adsorption/desorption stages initiated by a temperature jump, the procedure for heat transfer coefficients α_2 (flat layer) measuring is described in literature [23]. To determine α_2 the kinetic curves under quasi-isobaric conditions and different temperature driving force of the process ($\Delta T = T_{fin} - T_{init}$) should be measured (Fig. 4 orange arrows). It is important to note, that for adsorbents with a stepped sorption equilibrium curves (e.g. Figure 5a), T_{init} can be determined from the position of the step at the fixed pressure $T_{init} = T_d^*$ (Fig. 5 b, Fig. 4). Change in T_{fin} will result in different values of maximum power transferred from the adsorbent to the HTF through the area of adsorbent-metal contact:

$$W_{max} = \alpha_2 S \Delta T / m = \alpha_2 S (T_{fin} - T_{init}) / m \tag{4}$$

where m mass of the adsorbent, α_2 heat transfer coefficient between flat layer of the adsorbent and the metal support, S area of adsorbent-metal contact. The α_2 coefficient can be determined as the slope of the graph “maximal power W_{max}

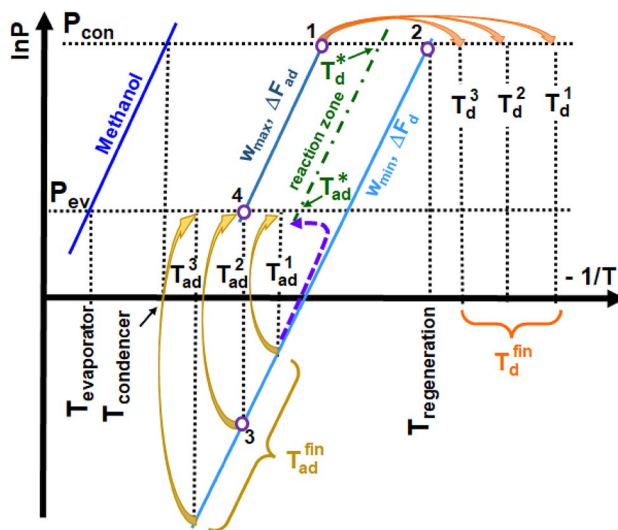


Fig. 4 Scheme for α_2 measurements: temperature jumps (orange arrows) and pressure jumps (yellow arrows). Adiabatic heating of adsorbent is showed by dashed arrow

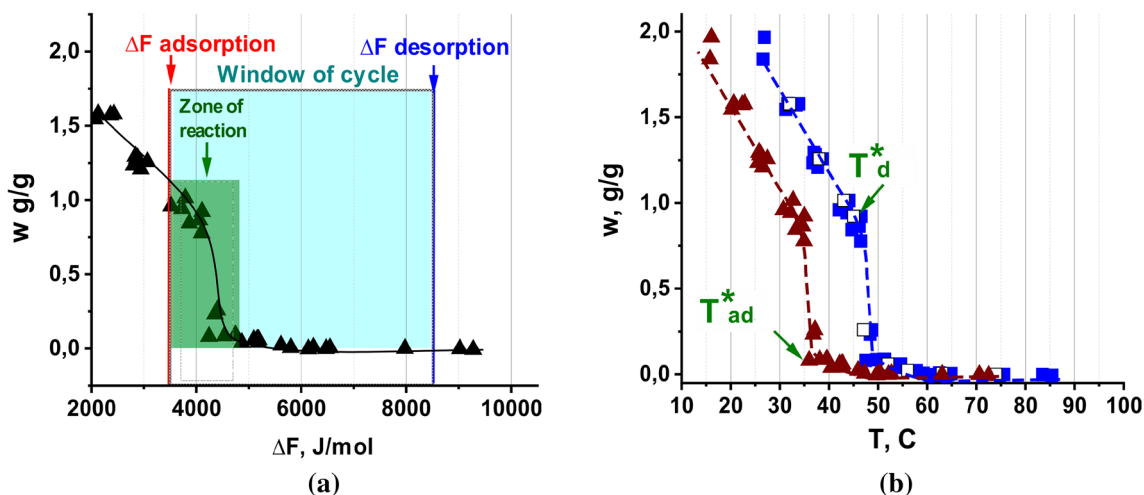


Fig. 5 **a** Boundary potentials of daily heat storage cycle and dependence of uptake “ w vs Polanyi potential ΔF ” for “LiCl/MWCNT—methanol” calculated using data of [33]; **b** Calculated (solid symbols) and measured in [33] (open symbols) isobars for the system “LiCl/MWCNT—methanol” at P_{ev} 55 mbar (blue closed square, closed square) and 96 mbar (brown triangle)

vs ΔT ”. After a number of experiments at different final desorption temperatures T_d^{fin} (T_d^1, T_d^2, T_d^3) (Fig. 4 orange arrows) α_2 for the adsorbent regeneration stage (Fig. 2 points 1–2) can be determined [23].

In case of heat generation, the adsorption stage is initiated by pressure jump (3–4 Fig. 2). Measurement of α_2 under such conditions is quite different from the abovementioned widespread LTJ technique. The main feature of the new technique is the assumption that after adsorption of the first portions of working liquid, the adiabatic heating of the adsorbent up to temperature T_{ad}^* occurs (Fig. 4, dashed arrow). After that temperature of the adsorbent decreases to T_{ad}^{fin} , which equals temperature of HTF circulating through AdHex channels. In other words, a thermal driving force appears due to pressure jump. This quite new method was approved and verified by comparison of experimental and theoretical results published in [41].

For composite materials “Salt inside porous matrix” characterized by a stepped isotherm [42] the reaction between the salt in the matrix pores and the vapors begins when the adsorbent reaches temperature T_{ad}^* (Fig. 5b). Taking this fact into consideration one can assume that the driving force of the reaction may be calculated as $\Delta T = T_{ad}^* - T_{ad}^{fin}$. For a number of different pressure jumps (Fig. 4 yellow arrows) different driving force values can be realized $\Delta T = T_{ad}^* - T_{ad}^{fin}$ ($T_{ad}^{fin}: T_{ad}^1, T_{ad}^2, T_{ad}^3$). Plotting the dependence of the maximum power versus ΔT make it possible finding α_2 coefficient (as a slope of the graph) for the heat release stage initiated by sharp pressure jump. The temperature T_{ad}^* can be found from the sorption equilibrium data of the working pair “LiCl/MWCNT—methanol” [33] (Fig. 5).

The boundary adsorption potentials of Polanyi ΔF determine the window of the adsorption heat storage cycle [43].

Amount of adsorbed liquid can be definitely determined as a function of only one parameter—the Polanyi potential $w = f(\Delta F)$. The Polanyi potential ΔF can be calculated as a function of the working cycle conditions ($T_{con}, T_{ev}, T_{reg}, T_{ad}, P_{con}, P_{ev}$). These parameters are determined by the climatic conditions of the region where the device will be used. The boundary potential ΔF_d related to the weak isostere (w_{min}) (stage 2–3 Figs. 2, 4) can be find according to the following expression:

$$\Delta F_d = -RT_{reg} \ln \left(\frac{P_{con}}{P^0(T_{reg})} \right), \tag{5}$$

where $P^0(T_{reg})$ —saturated pressure of methanol at the regeneration temperature T_{reg} .

The reach isostere (w_{max}) corresponds to the boundary potential ΔF_{ad} (stage 4–1 Figs. 2, 4). Adsorption potential in this case can be find using the following formula:

$$\Delta F_{ad} = -RT_{ad} \ln(P_{ev}/P^0(T_{ad})), \tag{6}$$

where $P^0(T_{ad})$ saturated pressure of methanol at temperature T_{ad} .

The boundary potentials (the window of cycle) and functional dependence $w = f(\Delta F)$ give the possibility to estimate amount of working liquid exchanged in the cycle by the adsorbent (Fig. 5) $\Delta w = w_{max} - w_{min}$. The chemical reaction between methanol and LiCl placed inside pores of matrix manifests itself on isobar as a step (Fig. 5). The reaction temperature T_{ad}^* can be found from the position of this step. In considered daily heat storage cycle, the saturation vapor pressure of working liquid is 55 mbar and 96 mbar at $T_{ev} = 5$ °C and $T_{con} = 15$ °C, respectively.

To estimate T_{ad}^* , one needs to use data about sorption isobars at appropriate pressures. These isobars can be recalculated from data array “ w vs ΔF ” [33]. The data from [33] should be recalculated into a data array “ w vs T ” at constant pressures equal to $P_{ev} = 55$ mbar and $P_{con} = 96$ mbar. To recalculate the data, it is necessary to rewrite the expression (6):

$$\Delta F_{ad} = -RT_{ad}(\ln(P_{ev}) - \ln(P^0(T_{ad}))), \quad (7)$$

To get saturation vapor pressure $P^0(T)$ of methanol Clausius–Clapeyron equation should be used:

$$\ln\left(\frac{P^0(T)}{(P = 1 \text{ atm})}\right) = -\frac{\Delta H^0}{R} * \left(\frac{1}{T} - \frac{1}{T_0}\right), \quad (8)$$

where T_0 boiling temperature of methanol at pressure $P = 1$ atm. The rewriting of (8) taking in mind that $T_0 = \text{constant}$ gives:

$$\ln(P^0(T)) = D + \frac{Q}{T}, \quad (9)$$

where Q and D are constants related to enthalpy and entropy characterizing evaporation of methanol. After combination of (7) and (9) and a number of mathematical transformations one can get final expression for T_{ad} :

$$\Delta F_{ad} = -RT_{ad}\left(\ln(P_{ev}) - \left(\frac{Q}{T_{ad}} + D\right)\right), \quad (10)$$

$$\Delta F_{ad} = -R(T_{ad}\ln(P_{ev}) - Q - T_{ad}D), \quad (11)$$

$$\frac{\Delta F_{ad}}{-R} + Q = T_{ad}(\ln(P_{ev}) - D), \quad (12)$$

$$T_{ads} = \left(\frac{\Delta F_{ad}}{-R} + Q\right) / (\ln(P_{ev}) - D), \quad (13)$$

Using the expression (13) it is possible to convert the array of “ w vs ΔF ”, into arrays of “ w from T ” at $P_{ev} = 55$ mbar and $P_{con} = 96$ (Fig. 5b). It is important to note that isobar for $P_{con} = 96$ mbar calculated from data published in [33] and isobar directly measured in [33] at the same pressure coincide (Fig. 5b). So, the proposed recalculation procedure can be used for building isobar at $P_{ev} = 55$ mbar (unfortunately such data are not presented in literature). From the position of the step on plotted isobars, it is evident that for heat release stage $T_{ad}^* \approx 36$ °C and for heat storage stage $T_d^* \approx 45$ °C (Fig. 5 b). These values of T^* and the measured values of the maximum power will serve for calculation of the α_2 coefficients for adsorption and desorption stages.

Materials and methods

Adsorbent synthesis

The procedure of the composite adsorbent LiCl/MWCNT preparation is described in detail in [33]. The multi-wall carbon nanotubes were synthesized and provided by the Laboratory of Surface Compounds Synthesis of the Boreskov Institute of Catalysis [44, 45]. Composite was synthesized by a wet impregnation method described in [33] using MWCNT as a matrix. Firstly, MWCNT were dried at 160 °C and immersed in excess of LiCl alcohol-aqueous solution with 1 h exposition time. The water-jet air pump was used to remove the solution excess by filtration. The sample was rinsed out with ethanol to remove the salt from the external surface of MWCNT globules and then dried at 160 °C for 12 h until the constant weight. From the difference in weight of the prepared composite and weight of initial matrix the salt concentration in the material was calculated and turned out to be as high as 41 wt.%. LiCl/MWCNT powder was pelleted using pressing during 30 s without any binder. The granules with the grain size of 0.4–0.5 mm were prepared from pellets by grinding and sieving. Texture characteristics of the prepared material were measured by a low-temperature nitrogen adsorption (NOVA 1200e): pore volume 2.7 cm³/g, surface area 145 m²/g. Scanning electron images were obtained with a microscope JEOL JSM-6460 (Fig. 6).

Heat transfer coefficients measurements

Heat transfer coefficient during adsorption stage

To measure α_2 coefficient under conditions of the adsorption stage the large pressure jump (LPJ) method was used (Fig. 7, blue circuit). The LPJ method gives a possibility to simulate in a laboratory the operation of a real adsorption heat accumulator.

Under conditions of heat release stage, methanol sorption was initiated by a pressure jump over the adsorbent. The support with monolayer of the adsorbent was maintained at a constant temperature. The pressure jump was organized by opening valve between the reactor with adsorbent (P_{init}) and the buffer tank (P_{fin}) (Fig. 7). After reaching the equilibrium pressure in the whole system is close to pressure in buffer tank (P_{fin}) because volume of buffer vessel is about 300 times larger than volume of the reactor. Pressure temporal evolution in the system was registered with the pressure gauge. The amount of adsorbed methanol was calculated according to ideal gas equation. In details method of adsorption kinetic measurements by pressure jump is described in [46].

Fig. 6 SEM images of MWCNTs (a) and LiCl/MWCNTs (b). Magnification 5:10,000

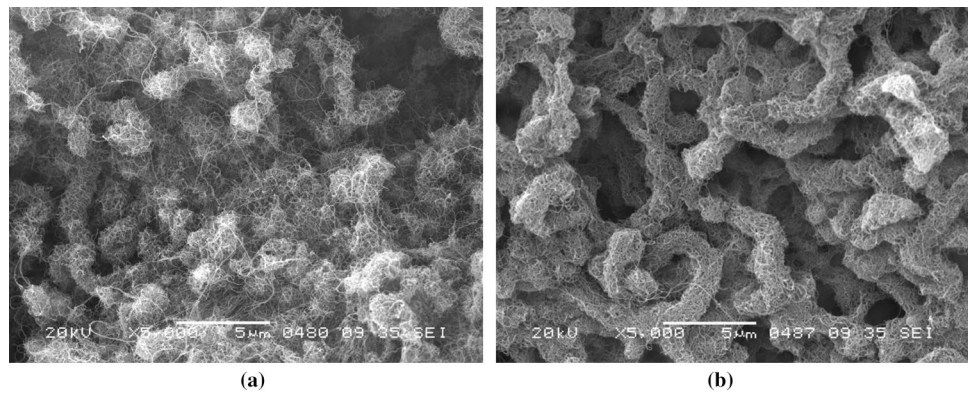
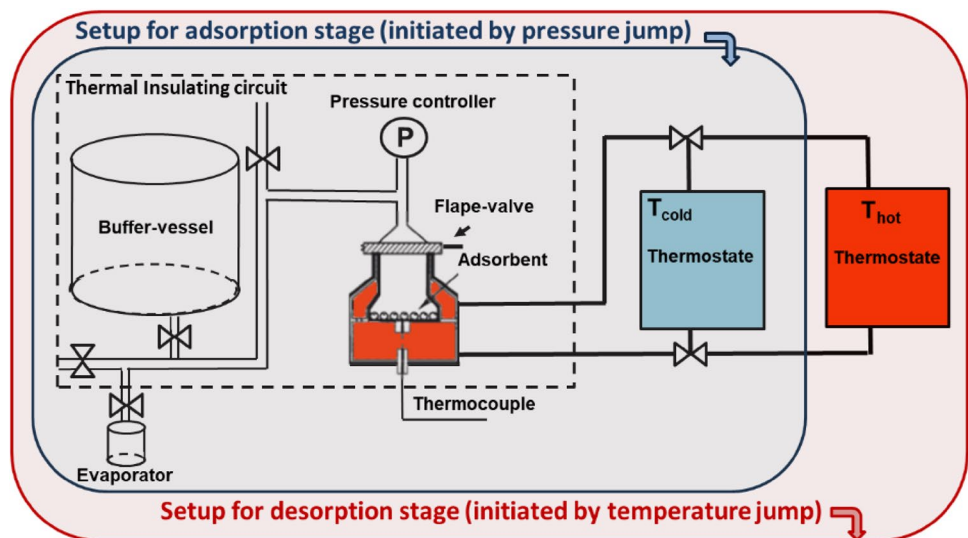


Fig. 7 Setup for α_2 measurement: adsorption stage (blue circuit) and desorption stage (red circuit)



As it was mentioned above, to calculate α_2 , a number of experiments at different adsorption temperatures (T_{ad}^1 , T_{ad}^2 , T_{ad}^3 etc. (Fig. 4 yellow arrows)) were carried out. Final pressure was fixed $P_{fin} = P_{ev} = 55$ mbar, that corresponds to saturated pressure of methanol at $T_{ev} = 5$ °C. Initial pressure P_{init} was 4, 5, 7, 9 mbar that corresponds $T_{ad}^{fin} = 20, 25, 30$, and 35 °C.

Heat transfer coefficient during desorption stage

In order to simulate desorption stage, method of Large temperature jump (LTJ) was used [22]. Desorption was initiated by sharp change in temperature of the metal support under the adsorbent by commutation with two thermostats at constant pressure $P_{con} = 96$ mbar (Fig. 7, red circuit). The initial temperature of desorption was 41 °C, the final temperature of desorption was varied $T_d^{fin} = 70, 75, 80$, and 85 °C. Configuration of granules was the same as in the adsorption experiment. Buffer vessel was connected with reactor during all time of the experiment supporting the quasi-isobaric conditions. Pressure temporal evolution in the system was registered with

the pressure gauge. The amount of adsorbed methanol was calculated according to ideal gas equation.

Results and discussion

Heat transfer coefficient for adsorption stage

The typical kinetic curves of methanol adsorption initiated by pressure jump are presented in Fig. 8. One can see that with a decrease in T_{ad}^{fin} , the driving force of the adsorption process $\Delta T = T_{ad}^* - T_{ad}^{fin}$ increases, which leads to a shorter time to reaching equilibrium. Thus, for the kinetic curve obtained at $T_{ad}^{fin} = 35$ °C, the conversion close to 1 is achieved in 1200 s, while for the curve obtained at $T_{ad}^{fin} = 30$ °C, the appropriate time is 500 s (Fig. 8a). The initial parts of considered curves obey an exponential equation:

$$q = \frac{w(t)}{w(t = \infty)} = 1 - \exp\left(-\frac{t}{\tau}\right), \quad (14)$$

Fig. 8 Kinetic curves for LiCl/ MWCNT—methanol at $P_{\text{fin}} = 55$ mbar and $T_{\text{ad}}^{\text{fin}}$: **a** 30 °C, (blue square) pressure jump from 7 mbar, 35 °C (square) pressure jump from 9 mbar; **b** (a) 20 °C (blue square), 25 °C (square). Experiment – symbols, red line – linear approximation

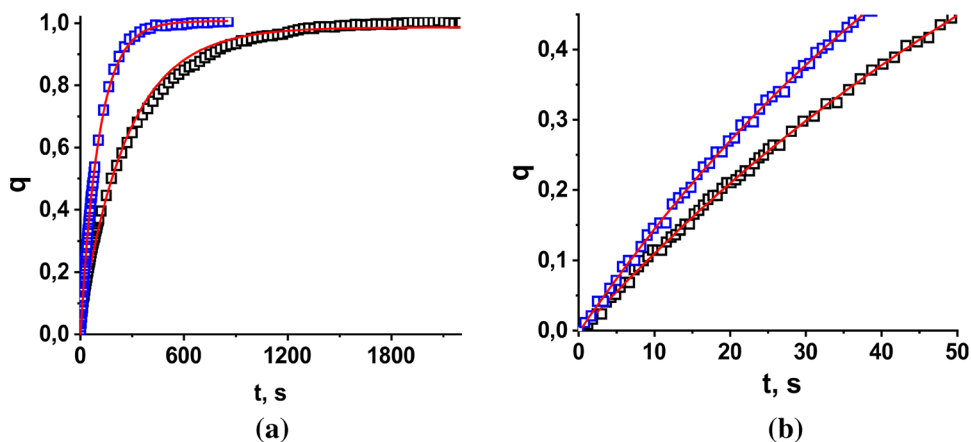
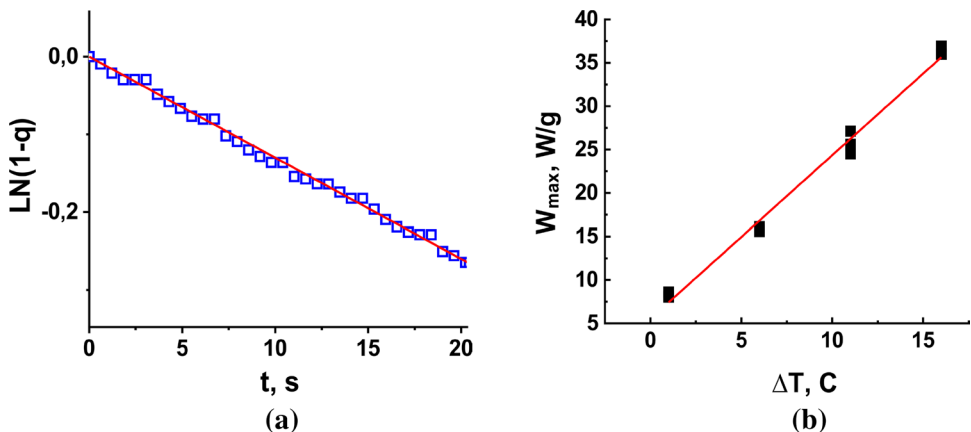


Fig. 9 **a** Initial part of kinetic curve in logarithmic coordinates for LiCl/MWCNT—methanol at $T_{\text{ad}}^{\text{fin}} = 25$ °C, pressure jump from 5 to 55 mbar; **b** maximum power vs ΔT . Experiment – symbols, red lines – linear approximation



where q conversion is a ratio of methanol amount adsorbed at time t to methanol amount adsorbed in equilibrium (at $t \rightarrow \infty$), τ —characteristic time of the process. Such behavior was found in the literature for various adsorbents such as salt in a porous matrix, coals, and also for various metal organic frameworks [16, 47–49].

In the experiments performed, the kinetic curves at lower temperatures $T_{\text{ad}}^{\text{fin}}$ (20, 25 °C) were restricted before reaching the full conversion. Indeed, at low adsorption temperature in case of reaching $q \approx 1$ the adsorbent would sorb a volume of liquid that exceeds the pore volume of the matrix. Thus, upon approaching to $q = 1$, the methanol solution of the salt would leak out of the pores, which would lead to sample deterioration. To avoid this scenario, the duration of the experiments was no more than 50 s and the conversion did not exceed 0.45 (Fig. 8b). The initial parts of these curves also obey exponential approximation (Fig. 8b). Using the Eq. (14) it is easy to find the characteristic time graphically as a slope of the initial part of the graph “ $\ln(1 - q)$ vs t ” (Fig. 9a, Table 1). Change in $T_{\text{ad}}^{\text{fin}}$ leads to change in the $\Delta T = T_{\text{ad}}^* - T_{\text{ad}}^{\text{fin}}$ value. Increasing of the adsorption temperature from 20 to 35 °C results in increase of characteristic time from 66 to 180 s (Table 1). As kinetic curve obeys the

Table 1 Characteristics of adsorption process at different $T_{\text{ad}}^{\text{fin}}$

$T_{\text{ad}}^{\text{fin}}, \text{C}$	$\Delta T, \text{C}$	τ, s	$W_{\text{max}}, \text{W/g}$
20	16	66	36.3 ± 0.5
25	11	81	25.7 ± 0.5
30	6	113	15.8 ± 0.5
35	1	180	8.3 ± 0.5

exponential equation maximum adsorption power can be found according to the formula:

$$W_{\text{max}(t=0)} = \Delta w * \Delta H * \frac{d\left(1 - \exp\left(-\frac{t}{\tau}\right)\right)}{dt} \Bigg|_{(t=0)} = \Delta w * \Delta H * \frac{1}{\tau} \quad (15)$$

where Δw – amount of methanol adsorbed in equilibrium under conditions of the cycle, ΔH is isosteric heat for methanol sorption by LiCl/MWCNT 47 ± 3 kJ/mol [33]. For granules with size 0.4–0.5 mm W_{max} is in the range of 8.3–36.3 W/g (Fig. 9b, Table 1).

Using the obtained data (Table 1) the heat transfer coefficient between metal and adsorbent was found from a slope of

the plot “ W_{\max} vs ΔT ” $\alpha_2 = 190 \pm 10 \text{ W}/(\text{m}^2\text{K})$. If α_2 is known, the global heat transfer coefficient UA of Hex with determined geometry can be estimated (1–3). For example, let’s consider heat exchanger with following geometrical parameters: primary surface area $A = 0.0264 \text{ m}^2$, area of the fins $A_f = 0.1281 \text{ m}^2$, height of the fins $h_f = 8 \text{ mm}$, thickness of the fins $\delta_f = 75 \text{ }\mu\text{m}$, fins pitch $\Delta_f = 1.7 \text{ mm}$, internal height of the channel $h'_{\text{ch}} = 1 \text{ mm}$, wall thickness $\delta_w = 0.5 \text{ mm}$. This Hex was described in details in [24]. For considered Hex loaded with composite LiCl/MWCNT granules 0.4–0.5 mm overall heat transfer coefficient U equals $833 \text{ W}/\text{m}^2\text{K}$. Thus, global heat transfer coefficient for abovementioned Hex $UA = 22 \text{ W}/\text{K}$. Taking into account that the Hex volume is 140 cm^3 , it is easy to estimate the volumetric thermal conductance of Hex with determined geometry as high as $157 \text{ W}/(\text{K}\cdot\text{dm}^3)$. From conditions of the cycle ($T_{\text{ad}} = 30\text{C}$ and $T_{\text{ev}} = 5\text{C}$) and sorption equilibrium data (Fig. 5b $T_{\text{ad}}^* = 36 \text{ }^\circ\text{C}$) temperature driving force realized in the adsorption stage (3–4, Fig. 2) can be found $\Delta T^* = 36 \text{ }^\circ\text{C} - 30 \text{ }^\circ\text{C} = 6 \text{ }^\circ\text{C}$. In this case it is easy to evaluate the volumetric maximum adsorption power generated during adsorption for considered Hex: $W_{\max}(\text{te or}) = UA \cdot \Delta T^* / V_{\text{Hex}} = 0.9 \text{ kW}/\text{dm}^3$. Thus, knowing α_2 and geometry of any FFT Hex one can easily estimate maximum power of the heat release stage for defined cycle.

Heat transfer coefficient for desorption stage

From Fig. 10a one can see that time needed for temperature jump from 41 to $80 \text{ }^\circ\text{C}$ of metal support is approximately 20 s . This very fast rise in temperature of metal support initiates desorption process. Data obtained from kinetic experiments are in good agreement with sorption equilibrium of the system LiCl/MWCNT—methanol (Fig. 5a). Indeed, according to sorption equilibrium data change in uptake Δw in the cycle equals $1.2 \text{ g}/\text{g}$. Approximately the same value of uptake change ($\Delta w = 1.2 \pm 0.1 \text{ g}/\text{g}$) one can observe for measured kinetic curve (Fig. 10a). In comparison with traditional adsorbent materials under the same cycle conditions this Δw value is impressive (for systems “microporous silica gel—water” [50] and “carbon MaxSorbIII—methanol” [51] Δw is about $0.066 \text{ g}/\text{g}$ and $0.6 \text{ g}/\text{g}$ respectively).

For $T_{\text{d}}^{\text{fin}} = 80 \text{ }^\circ\text{C}$ the initial part of kinetic curve obeys exponential Eq. (14) (Fig. 10b). The same behavior was observed for other desorption temperatures $T_{\text{d}}^{\text{fin}} = 70, 75, 85 \text{ }^\circ\text{C}$ (not presented). Using the Eq. (14) it is easy to find the characteristic time graphically from the slope of the initial part of the graph “ $\ln(1 - q)$ vs t ” (Fig. 11a, Table 2). The values of maximum power were found according to (15).

Fig. 10 Desorption kinetic curves for LiCl/MWCNT—methanol at $P_{\text{ev}} = 55 \text{ mbar}$, $T_{\text{d}}^{\text{fin}} = 80 \text{ }^\circ\text{C}$: **a** amount of methanol bound by the sorbent (symbols), temperature (line); **b** conversion (symbols), line – exponential approximation

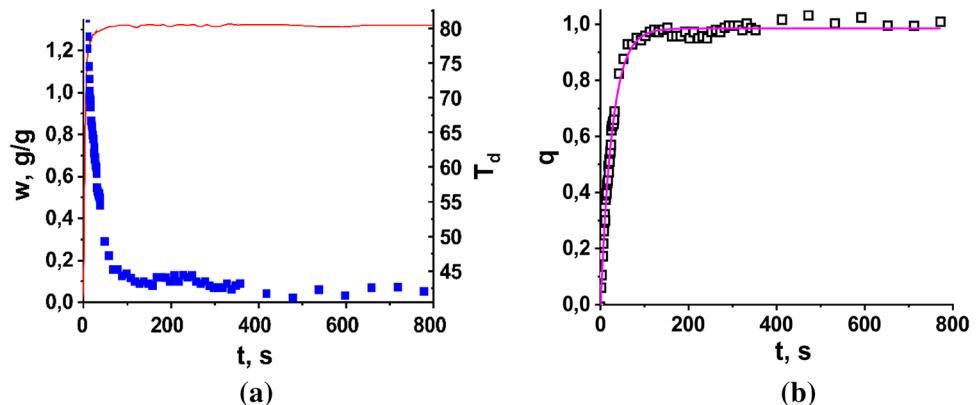


Fig. 11 **a** Initial part of kinetic curve in logarithmic coordinates for LiCl/MWCNT—methanol at $P_{\text{ev}} = 55 \text{ mbar}$, $T_{\text{d}}^{\text{fin}} = 80 \text{ }^\circ\text{C}$; **b** maximum power vs ΔT . Experiment – symbols, red lines – linear approximation

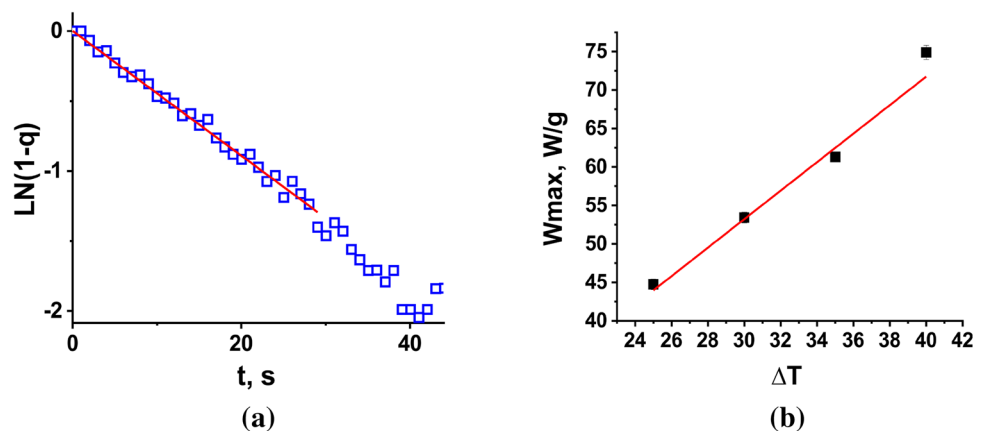


Table 2 Characteristic of desorption process for different T_d^{fin}

$T_d^{\text{fin}}, \text{C}$	$\Delta T, \text{C}$	τ, s	$W_{\text{max}}, \text{W/g}$
70	25	23	44.8 ± 0.7
75	30	28	53.4 ± 0.7
80	35	31	61.3 ± 0.7
85	40	37	74.9 ± 0.7

Again, increase in driving force results in increase of power generated during desorption stage. For granules with size 0.4–0.5 mm W_{max} for desorption stage lies in the range of 45–75 W/g (Fig. 11b, Table 2). It is important to note that regeneration of the system needs very short time. Indeed, Fig. 10b evidences that 10 min is more than enough for completing the desorption.

The heat transfer coefficient between metal and adsorbent for desorption stage was found from a slope of plot “ W_{max} vs ΔT ” $\alpha_2 = 170 \pm 10 \text{ W}/(\text{m}^2\text{K})$. The UA coefficient realized by abovementioned Hex in this case equals 20 W/K. This corresponds to volumetric conductance 146 W/(Kdm³). The temperature driving force can be found as $\Delta T^* = T_{\text{reg}} - T_d^* = 80 \text{ }^\circ\text{C} - 45 \text{ }^\circ\text{C} = 35 \text{ }^\circ\text{C}$. Using temperature driving force value one can theoretically estimate maximum power during desorption stage $W_{\text{max}}(\text{theor}) = UA \cdot \Delta T^* / V_{\text{Hex}} = 5.1 \text{ kW}/\text{dm}^3$.

Typical coefficients α_2 previously measured in works devoted to adsorbents under the conditions of adsorption heat transformation cycles are in the range of values from 100 to 200 W/K [16, 52, 53]. The heat transfer coefficients obtained in this work are in accordance with this range. It is interesting to note that the heat transfer coefficients for the stages of sorption and desorption for the “LiCl/MWCNT—methanol” system do not differ too much—the difference is about 10%. When comparing the obtained coefficients α_2 with the heat transfer coefficients obtained for the “LiCl/SiO₂—methanol” system in a similar cycle [41], one can say that for both systems the heat transfer coefficient at the sorption stage initiated by a pressure jump is higher than at the desorption stage initiated by a temperature jump. In general, α_2 obtained for the “LiCl/MWCNT—methanol” system is lower than the corresponding coefficients for the “LiCl/SiO₂—methanol” system for the adsorption stage (270 W/m²K [41]) and higher for the desorption one (130 W/m²K [41]). It is important to note that the estimated UA values per unit of Hex volume about 150 W/(Kdm³) are visibly higher than those reported in literature which is 50–100 W/(Kdm³) [54]. Taking into account the high value of the sorption capacity, the values of heat transfer coefficients exceeding 150 W/m²K for both the sorption and desorption stages, and the extremely short regeneration time of the adsorbent LiCl/MWCNT under cycle conditions, it is evident that the considered working

pair is promising for renewable energy storage and conversion by daily heat storage.

Conclusions

The paper considers the thermophysical characteristics of the working pair LiCl/MWCNT—methanol for the cycle of daily heat accumulation. For the heat release stage, the heat transfer coefficient was obtained using the large pressure jump method. For the heat storage stage, the large temperature jump method was applied. The value of α_2 at the sorption stage is 190 W/m²K, and at the desorption stage it is 170 W/m²K. With use of α_2 as a parameter, theoretical estimations of the maximum power that would be generated in a FFT heat exchanger of known geometry filled with the adsorbent LiCl/MWCNT under the conditions of a daily heat storage cycle were done. The maximal volumetric power during heat release was found to be as high as 0.9 kW/dm³. The volumetric conductance for the considered Hex filled with studied adsorbent is about 150 W/(Kdm³). The abovementioned characteristics of LiCl/MWCNT adsorbent demonstrates the perspective of using this material for sustainable energy applications.

Acknowledgements The work was supported by the Russian Science Foundation project 21-79-10183.

Data availability The data that support the findings of this study are available from the corresponding author, Dr. Alexandra Grekova, upon reasonable request.

Declarations

Conflict of interest The authors declare that they have no conflict of interest.

Open Access This article is licensed under a Creative Commons Attribution 4.0 International License, which permits use, sharing, adaptation, distribution and reproduction in any medium or format, as long as you give appropriate credit to the original author(s) and the source, provide a link to the Creative Commons licence, and indicate if changes were made. The images or other third party material in this article are included in the article's Creative Commons licence, unless indicated otherwise in a credit line to the material. If material is not included in the article's Creative Commons licence and your intended use is not permitted by statutory regulation or exceeds the permitted use, you will need to obtain permission directly from the copyright holder. To view a copy of this licence, visit <http://creativecommons.org/licenses/by/4.0/>.

References

1. Communication from the commission to the European parliament, the council, the European economic and social committee and the committee of the regions, Brussels, 16.02.2016. https://ec.europa.eu/energy/sites/ener/files/documents/1_EN_ACT_part1_v14.pdf
2. Camarasa, C., Mata, É., Navarro, J.P.J., et al.: A global comparison of building decarbonization scenarios by 2050 towards 1.5–2

- °C targets. *Nat. Commun.* **13**, 3077 (2022). <https://doi.org/10.1038/s41467-022-29890-5>
3. Zhang, X., Han, L., Wei, H., Tan, X., Zhou, W., Li, W., Qian, Y.: Linking urbanization and air quality together: a review and a perspective on the future sustainable urban development. *J. Clean. Prod.* **346**, 130988 (2022). <https://doi.org/10.1016/j.jclepro.2022.130988>
 4. Nassar, Y.F., Alsadi, S.Y., El-Khozondar, H.J., et al.: Design of an isolated renewable hybrid energy system: a case study. *Mater. Renew. Sustain. Energy* **11**, 225–240 (2022). <https://doi.org/10.1007/s40243-022-00216-1>
 5. Boulebbina, C., Mebarki, G., Rahal, S.: Passive solar house prototype design with a new bio-based material for a semi-arid climate. *Mater. Renew. Sustain. Energy* **11**, 1–15 (2022). <https://doi.org/10.1007/s40243-021-00203-y>
 6. Bourbia, S., Kazeoui, H., Belarbi, R.: A review on recent research on bio-based building materials and their applications. *Mater. Renew. Sustain. Energy* (2023). <https://doi.org/10.1007/s40243-023-00234-7>
 7. Wu, S.F., An, G.L., Wang, L.W., Zhang, C.: A thermochemical heat and cold control strategy for reducing diurnal temperature variation in the desert. *Sol. Energy Mater. Sol. Cells* **235**, 111460 (2022). <https://doi.org/10.1016/j.solmat.2021.111460>
 8. Calabrese, L., Bonaccorsi, L., Bruzzaniti, P., et al.: Adsorption performance and thermodynamic analysis of SAPO-34 silicone composite foams for adsorption heat pump applications. *Mater. Renew. Sustain. Energy* **7**, 24 (2018). <https://doi.org/10.1007/s40243-018-0131-y>
 9. Calabrese, L., Bruzzaniti, P., Palamara, D., Freni, A., Proverbio, E.: New SAPO-34-SPEEK composite coatings for adsorption heat pumps: adsorption performance and thermodynamic analysis. *Energy* **203**, 117814 (2020). <https://doi.org/10.1016/j.energy.2020.117814>
 10. Kocak, B., Fernandez, A.I., Paksoy, H.: Benchmarking study of demolition wastes with different waste materials as sensible thermal energy storage. *Sol. Energy Mater. Sol. Cells* **219**, 110777 (2021). <https://doi.org/10.1016/j.solmat.2020.110777>
 11. Navarro, M.E., Martínez, M., Gil, A., Fernández, A.I., Cabeza, L.F., Olives, R., Py, X.: Selection and characterization of recycled materials for sensible thermal energy storage. *Sol. Energy Mater. Sol. Cells* **107**, 131–135 (2012). <https://doi.org/10.1016/j.solmat.2012.07.032>
 12. Ye, C., Zhang, M., Yang, S., Mweemba, S., Huang, A., Liu, X., Zhang, X.: Application of copper slags in encapsulating high-temperature phase change thermal storage particles. *Sol. Energy Mater. Sol. Cells* **254**, 112257 (2023). <https://doi.org/10.1016/j.solmat.2023.112257>
 13. Devanuri, J.K., Gaddala, U.M., Kumar, V.: Investigation on compatibility and thermal reliability of phase change materials for low-temperature thermal energy storage. *Mater. Renew. Sustain. Energy* **9**, 24 (2020). <https://doi.org/10.1007/s40243-020-00184-4>
 14. Yu, N., Wang, R.Z., Wang, L.W.: Sorption thermal storage for solar energy. *Progr. Energy Comb. Sci.* **39**, 489–514 (2013). <https://doi.org/10.1016/j.pecs.2013.05.004>
 15. Chen, Z., Zhang, Y., Zhang, Y., Su, Y., Riffat, S.: A study on vermiculite-based salt mixture composite materials for low-grade thermochemical adsorption heat storage. *Energy* **278**, 127986 (2023). <https://doi.org/10.1016/j.energy.2023.127986>
 16. Gordeeva, L.G., Aristov, Yu.I.: Adsorptive heat storage and amplification: New cycles and adsorbents. *Energy* **167**, 440–453 (2019). <https://doi.org/10.1016/j.energy.2018.10.132>
 17. Lucia, U.: Adsorber efficiency in adsorption refrigeration. *Renew. Sustain. Energy Rev.* **20**, 570–575 (2013). <https://doi.org/10.1016/j.rser.2012.12.023>
 18. Jegede, O.O., Critoph, R.E.: Extraction of heat transfer parameters in active carbon–ammonia large temperature jump experiments. *Appl. Therm. Eng.* **95**, 499–505 (2016). <https://doi.org/10.1016/j.applthermaleng.2015.10.115>
 19. Palamara, D., Palomba, V., Calabrese, L., Frazzica, A.: Evaluation of ad/desorption dynamics of S-PEEK/Zeolite composite coatings by T-LTJ method. *Appl. Therm. Eng.* **208**, 118262 (2022). <https://doi.org/10.1016/j.applthermaleng.2022.118262>
 20. Papakokkinos, G., Castro, J., López, J., Oliva, A.: A generalized computational model for the simulation of adsorption packed bed reactors—parametric study of five reactor geometries for cooling applications. *Appl. Energy* **235**, 409–427 (2019). <https://doi.org/10.1016/j.apenergy.2018.10.081>
 21. Verde, M., Harby, K., Corberan, J.M.: Optimization of thermal design and geometrical parameters of a flat tube-fin adsorbent bed for automobile air-conditioning. *Appl. Therm. Eng.* **111**, 489–502 (2017). <https://doi.org/10.1016/j.applthermaleng.2016.09.099>
 22. Aristov, Y.I., Dawoud, B., Glaznev, I.S., Elyas, A.: A new methodology of studying the dynamics of water sorption/desorption under real operating conditions of adsorption heat pumps: experiment. *Int. J. Heat Mass Transf.* **51**, 4966–4972 (2008). <https://doi.org/10.1016/j.ijheatmasstransfer.2007.10.042>
 23. Gordeeva, L.G., Aristov, Yu.I.: Composite sorbent of methanol “LiCl in mesoporous silica gel” for adsorption cooling: dynamic optimization. *Energy* **36**, 1273–1279 (2011). <https://doi.org/10.1016/j.energy.2010.11.016>
 24. Grekova, A., Tokarev, M.: An optimal plate fin heat exchanger for adsorption chilling: theoretical consideration. *Int. J. Thermofl.* **16**(100221), 1–10 (2022). <https://doi.org/10.1016/j.ijtf.2022.100221>
 25. Feng, C., Jiaqing, E., Han, W., Deng, Y., Zhang, B., Zhao, X., Han, D.: Key technology and application analysis of zeolite adsorption for energy storage and heat-mass transfer process: a review. *Renew. Sustain. Energy Rev.* **144**, 110954 (2021). <https://doi.org/10.1016/j.rser.2021.110954>
 26. Piccoli, E., Brancato, V., Frazzica, A., Maréchal, F., Galmarini, S.: Adsorption energy system design and material selection: towards a holistic approach. *Therm. Sci. Eng. Prog.* **37**, 101572 (2023). <https://doi.org/10.1016/j.tsep.2022.101572>
 27. Calabrese, L., Brancato, V., Palomba, V., Frazzica, A., Cabeza, L.F.: Innovative composite sorbent for thermal energy storage based on a SrBr₂·6H₂O filled silicone composite foam. *J. Energy Storage* **26**, 100954 (2019). <https://doi.org/10.1016/j.est.2019.100954>
 28. Zhang, Y., Palomba, V., Frazzica, A.: Development and characterization of LiCl supported composite sorbents for adsorption desalination. *Appl. Therm. Eng.* **203**, 117953 (2022). <https://doi.org/10.1016/j.applthermaleng.2021.117953>
 29. Zhang, Y., Palamara, D., Palomba, V., Calabrese, L., Frazzica, A.: Performance analysis of a lab-scale adsorption desalination system using silica gel/LiCl composite. *Desalination* **548**, 116278 (2023). <https://doi.org/10.1016/j.desal.2022.116278>
 30. Adamu, H., Yamani, Z.H., Qamar, M.: Modulation to favorable surface adsorption energy for oxygen evolution reaction intermediates over carbon-tunable alloys towards sustainable hydrogen production. *Mater. Renew. Sustain. Energy* **11**, 169–213 (2022). <https://doi.org/10.1007/s40243-022-00214-3>
 31. Walle, M.D., Liu, Y.N.: Confine sulfur in double-hollow carbon sphere integrated with carbon nanotubes for advanced lithium–sulfur batteries. *Mater. Renew. Sustain. Energy* **10**, 1 (2021). <https://doi.org/10.1007/s40243-020-00186-2>
 32. Jahan, I., Rocky, K.A., Pal, A., Rahman, M.M., Saha, B.B.: A study on activated carbon and carbon nanotube based consolidated composite adsorbents for cooling applications. *Therm. Sci. Eng. Prog.* **34**, 101388 (2022). <https://doi.org/10.1016/j.tsep.2022.101388>
 33. Grekova, A.D., Gordeeva, L.G., Aristov, Y.I.: Composite sorbents “Li/Ca halogenides inside multi-wall carbon nano-tubes”

- for thermal energy storage. *Sol. Energy Mater. Sol. Cells* **155**, 176–183 (2016). <https://doi.org/10.1016/j.solmat.2016.06.006>
34. Brancato, V., Gordeeva, L.G., Grekova, A.D., Sapienza, A., Salvatore, V., Frazzica, A., Aristov, Y.I.: Water adsorption equilibrium and dynamics of LiCl/MWCNT/PVA composite for adsorptive heat storage. *Sol. Energy Mater. Sol. Cells* **193**, 133–140 (2019). <https://doi.org/10.1016/j.solmat.2019.01.001>
 35. Aristov, Yu.I.: Novel materials for adsorptive heat pumping and storage: screening and nanotailoring of sorption properties. *J. Chem. Eng. Jpn.* **40**, 1241–1251 (2007)
 36. Grekova, A.D., Gordeeva, L.G., Lu, Z., Wang, R., Aristov, Y.I.: Composite “LiCl/MWCNT” as advanced water sorbent for thermal energy storage: sorption dynamics. *Sol. Energy Mater. Sol. Cells* **176**, 273–279 (2018). <https://doi.org/10.1016/j.solmat.2017.12.011>
 37. Aristov, Yu.I.: Optimal adsorbent for adsorptive heat transformers: dynamic considerations. *Int. J. Refrig.* **32**, 675–686 (2009). <https://doi.org/10.1016/j.ijrefrig.2009.01.022>
 38. Rohsenow, W.M., Hartnett, J.P., Cho, Y.I.: *Handbook of heat transfer/editors*, 3rd edn. McGraw-Hill (1998)
 39. Ezgi, C.: Basic design methods of heat exchanger. In: Murshed, S.S., Lopes, M.M. (eds.) *Heat exchangers—design, experiment and simulation*. IntechOpen, London (2017)
 40. Erdoğan, M.E., Imrak, C.E.: The effects of duct shape on the Nusselt number. *Math. Computat. Appl.* **10**, 79–88 (2005). <https://doi.org/10.3390/mca10010079>
 41. Grekova, A., Strelowa, S., Solovyeva, M., Tokarev, M.: Adsorption heat storage: measurement of heat transfer coefficients in a metal-sorbent system during the heat release stage initiated by a pressure jump. In: 1430th International Conference on Civil and Environmental Engineering (ICCEE) will be held on 12th–13th August, 2023 at Cairo, Egypt (submitted) (2023)
 42. Lu, Z.S., Wang, R.Z.: Study of the new composite adsorbent of salt LiCl/silica gel-methanol used in an innovative adsorption cooling machine driven by low temperature heat source. *Renew. Energy* **63**, 445–451 (2014). <https://doi.org/10.1016/j.renene.2013.10.010>
 43. Polanyi, M.: Section III—theories of the adsorption of gases, A general survey and some additional remarks. Introductory paper to section III. *Trans. Faraday Soc.* **28**, 316–333 (1932)
 44. Rabinovich, O., Tsytsenka (Blinova), A., Kuznetsov, V., Moseenkov, S., Krasnikov, D.: A model for catalytic synthesis of carbon nanotubes in a fluidized-bed reactor: effect of reaction heat. *Chem. Eng. J.* **329**, 305–311 (2017). <https://doi.org/10.1016/j.cej.2017.06.001>
 45. Gribov, E.N., Kuznetsov, A.N., Golovin, V.A., et al.: Effect of modification of multi-walled carbon nanotubes with nitrogen-containing polymers on the electrochemical performance of Pt/CNT catalysts in PEMFC. *Mater. Renew. Sustain. Energy* **8**, 7 (2019). <https://doi.org/10.1007/s40243-019-0143-2>
 46. Sapienza, A., Frazzica, A., Freni, A., Aristov, Y.: Measurement of adsorption dynamics: an overview. *Springer Briefs Appl. Sci. Tech.* (2018). <https://doi.org/10.1007/978-3-319-51287-72>
 47. Girnuk, I.S., Okunev, B.N., Aristov, Yu.I.: Dynamics of pressure- and temperature-initiated adsorption cycles for transformation of low temperature heat: flat bed of loose grains. *Appl. Therm. Eng.* **165**, 114654 (2020). <https://doi.org/10.1016/j.applthermaleng.2019.114654>
 48. Han, B., Chakraborty, A.: Experimental investigation for water adsorption characteristics on functionalized MIL-125 (Ti) MOFs: enhanced water transfer and kinetics for heat transformation systems. *Int. J. Heat Mass Trans.* **186**, 122473 (2022). <https://doi.org/10.1016/j.ijheatmasstransfer.2021.122473>
 49. Rupam, T.H., Tuli, F.J., Jahan, I., Palash, M.L., Chakraborty, A., Saha, B.B.: Isotherms and kinetics of water sorption onto MOFs for adsorption cooling applications. *Therm. Sci. Eng. Prog.* **34**, 101436 (2022). <https://doi.org/10.1016/j.tsep.2022.101436>
 50. Aristov, Y.I., Tokarev, M.M., Freni, A., Glaznev, I.S., Restuccia, G.: Kinetics of water adsorption on silica Fuji Davison RD. *Microp. Mesop. Mat.* **96**, 65 (2006). <https://doi.org/10.1016/j.micromeso.2006.06.008>
 51. El-Sharkawy, I.I., Hassan, M., Saha, B.B., Koyama, S., Nasr, M.M.: Study on adsorption of methanol onto carbon based adsorbents. *Int. J. Refrig.* **32**, 1579 (2009). <https://doi.org/10.1016/j.ijrefrig.2009.06.011>
 52. Girnuk, I.S., Aristov, Yu.I.: Dynamic optimization of adsorptive chillers: the “AQSOA™-FAM-Z02—Water” working pair. *Energy* **106**, 13–22 (2016). <https://doi.org/10.1016/j.energy.2016.03.036>
 53. Aristov, Y.I., Glaznev, I.S., Girnuk, I.S.: Optimization of adsorption dynamics in adsorptive chillers: loose grains configuration. *Energy* **46**, 484–492 (2012). <https://doi.org/10.1016/j.energy.2012.08.001>
 54. Schnabel, L., et al.: Innovative adsorbent heat exchangers: design and evaluation. In: Bart, H.J., Scholl, S. (eds.) *Innovative heat exchangers*. Springer, Cham (2018). https://doi.org/10.1007/978-3-319-71641-1_12